CNR Dependence on Spatial Resolution and Subject Contrast in Phase Contrast CT

Brandon Nelson, Shuai Leng, and Cynthia McCollough
Mayo Clinic, Rochester, MN

CT Clinical Innovation Center

JULY 12–16 2020 VIRTUAL JOINT AAPM | COMP MEETING
EASTERN TIME [GMT-4]

INTRODUCTION

X-RAY PHASE CONTRAST

Grating-based imaging methods bring novel phase ϕ and visibility V x-ray contrasts to preclinical lab CT systems in addition to traditional absorption contrast μ

Phase ϕ: apparent improved soft-tissue contrast with potential applications in breast imaging (1)

Visibility V: sensitive to porous materials with potential application in lung imaging (1)

CONTRAST PROPERTIES

Each specific contrast depends on several factors including the **imaging system**

Previous simulation work has shown how imaging system parameters affect phase contrast CT contrast-to-noise ratio (CNR) compared to attenuation CT (2)

- Found noise properties of phase contrast support use for high resolution imaging (2-4)
- Simulations limited to monochromatic beam and makes assumptions about several system parameters and imaged materials

MOTIVATION

- Most practical systems use polychromatic beams and have other non-idealities
- Additionally, how is visibility contrast affected by imaging system parameters?

AIM

- Investigate CNR relationships with changing detector pixel size between grating-based contrasts in our experimental system with a polychromatic beam
- Compare to monochromatic predictions

METHODS

IMAGING SYSTEM

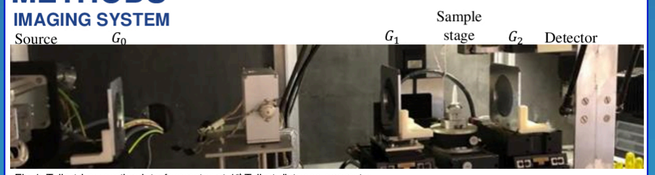

Fig 1. Talbot-Lau grating interferometer at 1st Talbot distance geometry.

Experiments performed using a Talbot-Lau grating interferometer benchtop micro CT (Fig. 1) operated at 40 keV mean energy with reference Talbot carpet visibility = 16 %.

- $G_0 - G_1$distance: 50 cm, $G_1 - G_2$ distance: 25 cm (d Eq. 2)

IMAGED SAMPLE

- Murine lung sample fixated and air inflated to end inspiration volume to maintain air-tissue contrast (Fig. 2).

Fig. 2. Air inflated fixed murine lung sample

IMAGE ACQUISITION

- Micro CT acquisitions retrospectively binned to vary detector size
- Each scan performed at 20, 30, 35 mAs and repeated twice for noise investigation

ANALYSIS

- ROIs taken from a heart region and lung along with nearby air ROI for background (bg)

$\mathrm{CNR}_\mu = \frac{|\mu_{ROI} - \mu_{bg}|}{\sigma_\mu}$, $\mathrm{CNR}_\phi = \frac{|\phi_{ROI} - \phi_{bg}|}{\sigma_\phi}$, σ = standard deviation of bg.

RESULTS

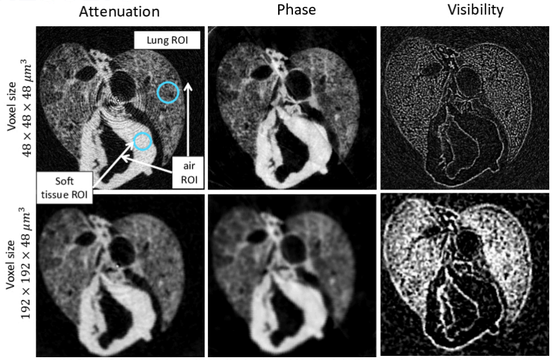

Fig 3. Attenuation, phase, and visibility images reconstructed at native and binned detector pixels. Display window/level $[mm^{-1}]$, $\mu = 0.005/0.0025$, $\phi = 0.03/0.015$, $V = 0.005/0.0025$.

CONTRAST MEASUREMENTS

ROI measurements used shown in Fig. 3 above

- Attenuation and phase contrast remains constant with detector binning (Fig. 4 above).
- Visibility contrast **increases** with pixel size

NOISE MEASUREMENTS

Repeat scans subtracted for noise analysis shown in Fig. 5 below.

- Noise power spectra (Fig. 6 at right) shows reduction of high frequency noise content in attenuation and visibility contrasts with larger detectors
- Phase noise content lower frequency and thus less effected by binning
- As a result, attenuation and visibility noise decrease with detector binning at greater rate than phase (Fig. 7).

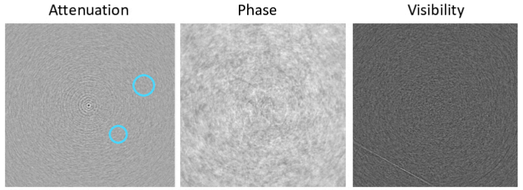

Fig 5. Measured noise images from subtracting repeat micro-CT scans used for calculating noise-power-spectrum (NPS)

CONTRAST TO NOISE RELATIONSHIPS

Contrast and noise relationships from Figs. 4-6 leads to CNR ratio curves in Fig. 8., enabling CNR comparisons as a function of detector size

- **Breakeven points**

Defined as detector pixel size where $CNR_\phi = CNR_V$

- Fitting curves to Fig. 8 plots enables experimental determination of breakeven points in Table 2.
- Repeated for 3 different mA yielded consistent results

- **Visibility trends**
  - Increasing contrast and decreasing noise results in increasing relative visibility CNR performance with pixel size

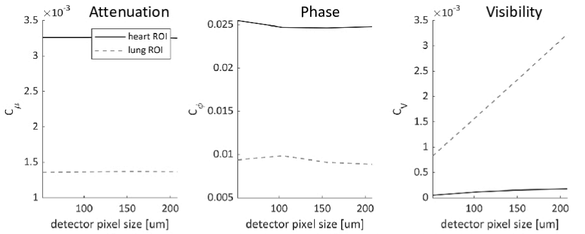

Fig 4. Measured contrast in select tissue ROIs as a function of binned detector size.

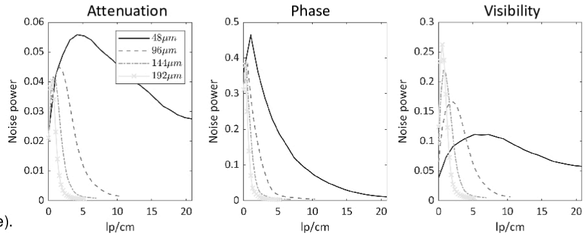

Fig 6. Noise power spectra acquired from soft tissue ROI in subtracted repeat scan noise image.

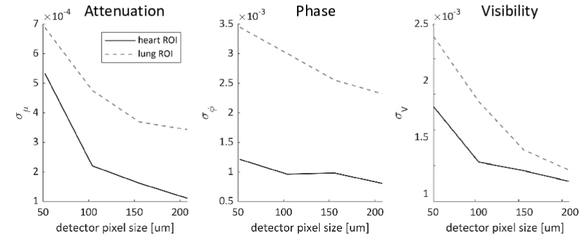

Fig 7. Measured noise as a function of binned detector size. Detector pixel size is in-plane voxel side length with slice thickness kept constant at 48 μm.

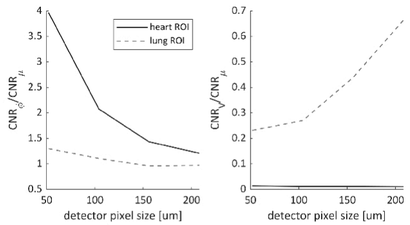

Fig 8. CNR ratios of phase and visibility over attenuation CNR plotted against detector pixel size. Table 2 at right shows phase transition points where phase CNR > attenuation CNR.

Pixel size where $\frac{CNR_\phi}{CNR_\mu} > 1$	
Soft Tissue	
mA	Voxel side length [μm]
35	250
30	250
25	270
Lung	
mA	Voxel side length [μm]
35	140
30	160
25	120

Table 2: Breakeven points for different tissues found for phase contrast. All binned detector sizes with side lengths ***less than*** the listed transition point have greater CNR in that material

DISCUSSION

CNR PERFORMANCE BETWEEN CONTRASTS

- Phase contrast advantaged with smaller pixel sizes due to low frequency noise content
- Visibility CNR improves with larger pixel sizes due to increasing contrast combined with higher frequency noise content

COMPARISON TO PREDICTED PHASE CNR BREAKEVEN POINTS

- In soft tissue, observed at pixel size $250\ \mu m$ $CNR_\phi = CNR_\mu$ in our experimental polychromatic setup
- Greater than the 212 μm predicted by monochromatic simulations (2)

VISIBILITY CONTRAST TRENDS

- Observed increasing visibility trends with larger pixel sizes due to similar noise characteristics as absorption contrast
- In given sample and system geometry
- Visibility, whose contrast derives from structure, is fundamentally different from phase and attenuation which derives from material properties
- Future work in quantifying visibility CNR performance requires using samples of varying local structure

LIMITATIONS

- Noise measurements in anatomic backgrounds
- Reconstructed visibility images in laboratory setups with polychromatic, large focal spot and detector period are susceptible to imaging system bias (5).

CONCLUSION

- Established relationships between three grating-based contrasts in our experimental system
- Results provide additional evidence supporting the use of phase contrast for high resolution soft tissue imaging

ACKNOWLEDGEMENTS

The authors thank Jeffrey Meridew, Nunzia Caporarello Ph.D., and Daniel Tschumperlin Ph.D. for their help providing the murine sample used and Andrea Bracchetti for his help in performing the fixation. This work was funded by Mayo Clinic ASU Team Science Award. This work was supported in part by the Mayo Clinic X-ray Imaging Research Core. We acknowledge the support of the CT Clinical Innovation Center and the Mayo Clinic Graduate School of Biomedical Sciences.

REFERENCES

1. Bravin A, Coan P, Suortti P. X-ray phase-contrast imaging: from pre-clinical applications towards clinics. Phys Med Biol. 2013;58(1):R1-35.
2. Raupach R, Flohr TG. Analytical evaluation of the signal and noise propagation in x-ray differential phase-contrast computed tomography. Phys Med Biol. 2011;56(7):2219-44.
3. Chen GH, Zambelli J, Li K, Bevins N, Qi Z. Scaling law for noise variance and spatial resolution in differential phase contrast computed tomography. Med Phys. 2011;38(2):584-8.
4. Kohler T, Jurgen Engel K, Roessl E. Noise properties of grating-based x-ray phase contrast computed tomography. Med Phys. 2011;38 Suppl 1:S106.
5. Koenig T, Zuber M, Trimborn B, Farago T, Meyer P, Kunka D, et al. On the origin and nature of the grating interferometric dark-field contrast obtained with low-brilliance x-ray sources. Phys Med Biol. 2016;61(9):3427-42.

CONTACT INFORMATION

Nelson.Brandon@Mayo.edu